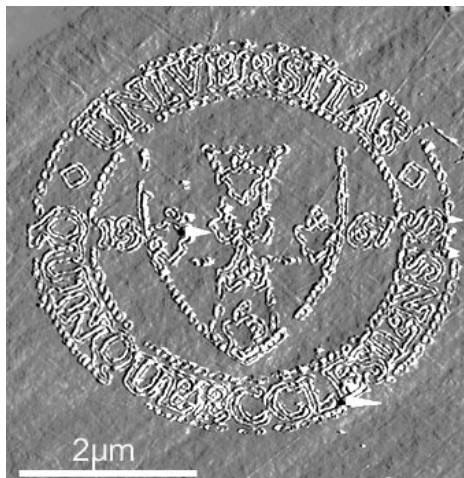


**Ph.D. Thesis**

**ATOMIC FORCE MICROSCOPY INVESTIGATION OF  
MORPHOLOGY AND NANOMECHANICAL PROPERTIES  
OF A $\beta$ -AMYLOID FIBRILS**

**Árpád Karsai M.D.**



**University of Pécs  
Faculty of Medicine  
Department of Biophysics**

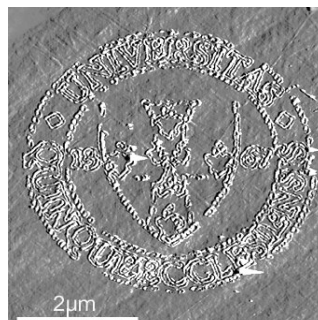
**2008**

# Ph.D. Thesis

## Atomic force microscopy investigation of morphology and nanomechanical properties of A $\beta$ -amyloid fibrils

**Árpád Karsai M.D.**

Program: Biochemistry and molecular biology  
Program leader: Dr. Balázs Sümegi  
Subprogram B-130: Investigation of functional protein dynamics with biophysical methods  
Subprogram leader: Dr. Béla Somogyi  
Dr. Miklós Nyitrai  
Supervisor: Dr. Miklós Kellermayer



University of Pécs  
Faculty of Medicine  
Department of Biophysics

## INTRODUCTION

Amyloidosis is a severe, usually fatal clinical disorder in which insoluble filamentous aggregates called amyloid fibrils are deposited in the extracellular space of various tissues. Amyloid fibrils are self-associating filamentous structures formed from various misfolded peptides and proteins. About 23 unrelated peptides have been reported to generate amyloid fibrils *in vivo*. Considering that there is no evidence for the development of amyloidosis in the absence of fibrillar deposits, the extracellular accumulation of amyloid fibrils is considered to be the most important factor in the pathogenesis of the disease.

Probably the most prominent and frequent form of amyloidosis is Alzheimer's disease. Alzheimer's disease was first described by Alois Alzheimer in 1907. The disease is manifested in cognitive and memory deterioration, progressive impairment of activities of daily living, and a variety of neuropsychiatric and behavioral disturbances. Since the incidence of Alzheimer's disease increases progressively with age, and the gradual increase of average age in developed countries, there has been a great interest in the better understanding of the mechanisms of amyloid fibril formation and in seeking profound therapeutic strategies for reducing the severity of the disease. .

A $\beta$ -protein, the main component of Alzheimer's amyloid  $\beta$ -fibrils (A $\beta$ -fibrils), was the first protein to be extracted from amyloid deposits. In recent years several, sometimes unexpected, proteins have also been shown to form amyloid fibrils. Because amyloid is thought to form as a consequence of improper folding of the particular protein, amyloidosis and its related diseases are also called misfolding diseases.

Amyloid fibrils are self-associating filamentous structures formed from the 39–43-residue-long amyloid  $\beta$ -peptide (A $\beta$ ) or its subfragments. The deposition of amyloid oligomers and fibrils is considered to be one of the most important factors in the pathogenesis of Alzheimer's disease and other disorders. The exact structure, dynamics, and the mechanisms of the amyloid fibrils' formation and cellular effects are not clearly understood.

## STRUCRURE OF AMYLOID FIBRILS

For long the structure of A $\beta$ -fibrils has for long been enigmatic because of insoluble aggregate formation that precludes the use of standard structural methods such as x-ray crystallography and solution NMR. Recent data from site-directed spin labeling, and particularly from solid-state NMR experiments, have formed the basis of a high resolution

model of the A $\beta$ 1–40 fibril:  $\beta$ -hairpins lying perpendicular to the fibril axis are associated into  $\beta$ -sheets that line up to form protofilaments, which are then assembled parallel into fibrils (Fig 1.).

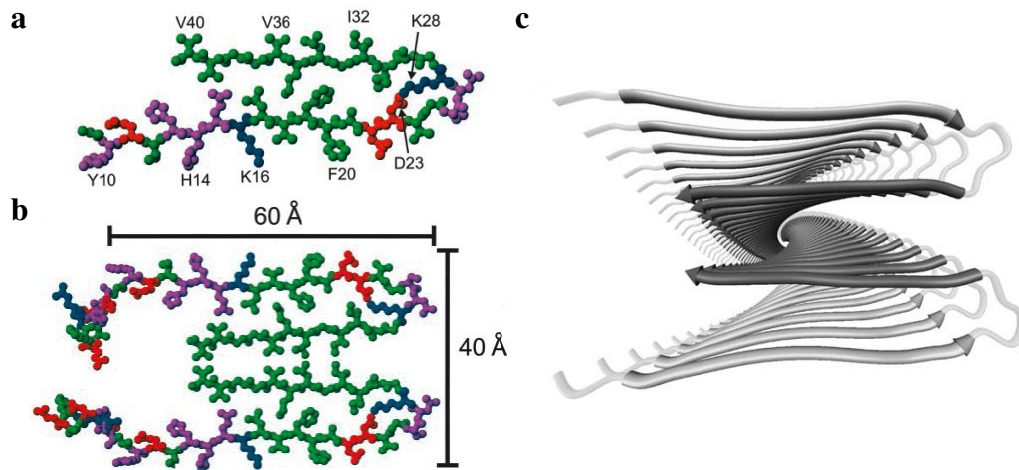


**Fig 1. A. and B.** Cross section of an A $\beta$ 1–40 fibril . **C.** Structural model for A $\beta$ 1–40 fibrils

Protofilaments are thus thought to represent an 2–3-nm-diameter structural unit within the amyloid fibril (Fig. 2.). During amyloidogenesis the formation of fibrils is preceded by the appearance of globular aggregates that are thought to fuse, by not fully understood mechanisms, into fibrillar structures. Recently, curved, beaded, 200-nm-long and 6–8-nm-wide fibrillar precursors were described to appear in the amyloidogenetic pathway, which were called protofibrils. The protofibrils are thought to go through a structural transition on their way to forming the amyloid fibril. The exact nature of structural dynamics within the amyloid fibril during amyloidogenesis, however, remains to be resolved.

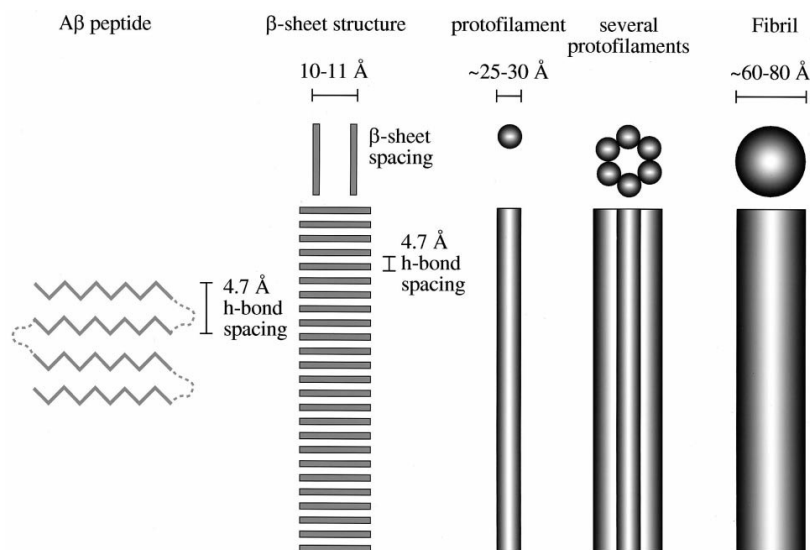


**Fig. 2.** The hierarchy of structure from the A $\beta$  peptide folded into a  $\beta$ -pleated sheet structure through protofilaments to amyloid fibrils.

## INVESTIGATION OF AMYLOID FIBRILS WITH ATOMIC FORCE MICROSCOPY

The atomic force microscopy (AFM) has been extensively utilised to study amyloid fibrils and aggregates in the last decade. This technique has made possible many advances to understand the behavior of the process of amyloidogenesis. The greatest achievement of the AFM is the possibility to study amyloids in a hydrated environment and enabling the visualisation of dynamic events like the nucleation of the amyloid protein or peptides and fibril formation and aggregation.

The AFM can take images in solution at distinct time points as well as generating time-lapse images about the initial steps of amyloid formation like seed formation and about growing fibrils and about the development of matured aggregates. With this technique it is possible to study the rates of fibrillogenesis, as well as mapping the progression of variations in morphologies and the development of structural hierarchy. Furthermore, events can be studied under conditions close to the native physiological state.

## NANOTECHNOLOGICAL APPLICATIONS OF AMYLOIDS

A special advantage of amyloid peptides is that variants suitable for a particular application may be generated by chemical or biotechnological methods. Once the fibrils are formed, they possess high stability under relatively harsh physical and chemical conditions. For nanotechnology applications, well-controlled orientation and growth of the fibrils are also desirable. A preferential orientation of A $\beta$ 1–42 sheets has been observed on a graphite surface. In the presence of the biogenic polyamine putrescine the oriented growth of  $\alpha$ -synuclein sheets on mica has been found. Partial, radial fibril orientation can be observed in

amyloid spherulites. Furthermore, amyloid plaques themselves may be considered as partially ordered assemblies of fibrils. However, the general global disorder in amyloid fibrillar arrangements currently stands in the way of their widespread use in nanotechnology applications.

## AIMS

1. Characterise the morphology of A $\beta$ 25-35, A $\beta$ 25-35\_G25Ac, A $\beta$ 25-35\_K28Ac, A $\beta$ 1-40 and A $\beta$ 1-42 amyloid fibrils with atomic force microscopy.
2. Characterise the nanomechanical behavior and nanomechanical fingerprint of A $\beta$ 25-35, A $\beta$ 25-35\_G25Ac, A $\beta$ 25-35\_K28Ac A $\beta$ 1-40 and A $\beta$ 1-42 amyloid fibrils with In-Situ force spectroscopy.
3. Characterise the orientated arrangement, morphology, binding properties and behavior of A $\beta$ 25-35, A $\beta$ 25-35\_G25Ac, and A $\beta$ 25-35\_K28Ac fibrils on mica.
4. Investigate the development of single A $\beta$ 25-35 and A $\beta$ 1-42 fibrils on mica and HOPS surface respectively with scanning-force kymography.

## RESULTS AND DISCUSSION

### MORPHOLOGY AND NANOMECHANICS OF A $\beta$ -FIBRILS

#### NANOMECHANICAL PROPERTIES OF A $\beta$ -FIBRILS

Amyloid fibrils formed from A $\beta$ 1–40 or A $\beta$ 25–35 peptides were mechanically manipulated using single molecule AFM. The fibrils were covalently attached to the surface. The force and extension data collected during the stretch-relaxation cycles provided a description of the mechanical response of the fibrils. The mechanical behavior of the two different amyloid fibrils was qualitatively similar.

Two fundamental types of mechanical responses were deduced: (a) fully reversible, non-linear elasticity (Fig. 3A) with the contour length often exceeding 100 nm, and (b) force plateau characterized with a constant force level during stretch (Fig. 3B). During extension the force plateau was sometimes preceded with a non-linear elastic response (Fig. 3B, inset) and usually ended with an abrupt force drop. Most frequently the two fundamental processes were combined into complex, hierarchical mechanical responses: force plateaus were superimposed onto one another (Fig. 3C) or onto a non-linear force curve (Fig. 3D). Superimposed force plateaus usually ended with a series of decreasing force steps resulting in a descending staircase pattern.

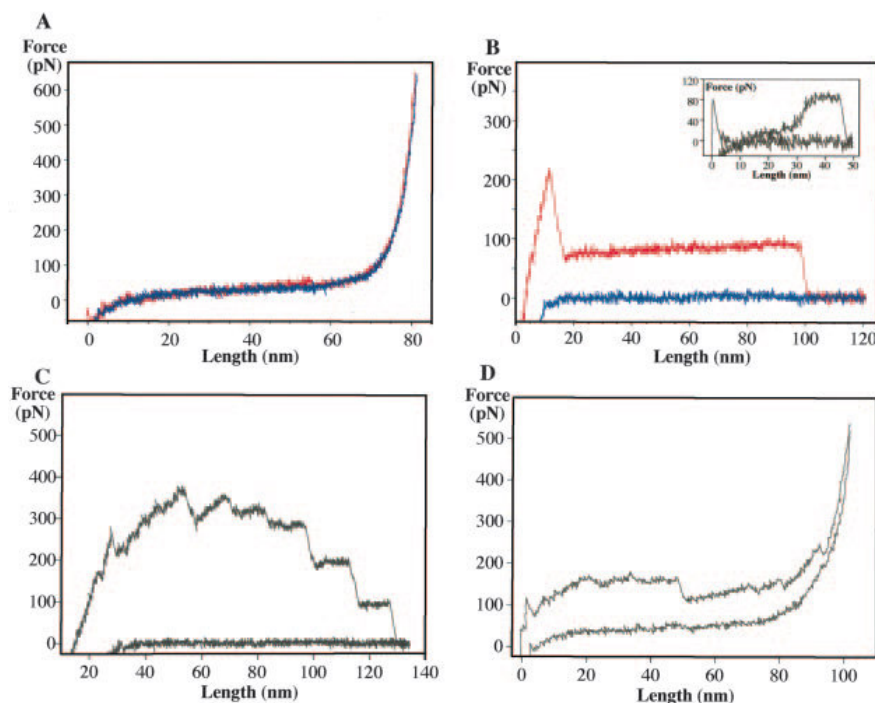


**Fig. 3.** Various force responses of mechanically manipulated A $\beta$ -fibrils. **A**, example of pure non-linear elasticity observed in A $\beta$ -fibrils. **B**, example of single force plateau. Inset, force plateau preceded by elastic response. The initial nonlinear elastic force curve merges into a force plateau. **C**, several force plateaus superimposed onto one another, forming a descending staircase. **D**, force plateaus and staircase superimposed onto non-linear elastic response.

Our results suggested that the mechanical response is determined by the elasticity and interactions of an element within the structural hierarchy of the mature A $\beta$ -fibril. These complex mechanical responses can be most plausibly explained by a reversible unzipping of long elastic  $\beta$ -sheets from the fibril.

## NANOMECHANICAL FINGERPRINT OF A $\beta$ -FIBRILS

We measured the height of the plateaus to determine the force which is needed for unzipping of long elastic  $\beta$ -sheets from the A $\beta$ -fibrils. The plateau force histograms revealed multimodal distribution for A $\beta$ 25–35 (Fig. 4A, ii) and pointed to multimodality for A $\beta$ 1–40 (Fig. 4A, i). The peaks corresponding to the smallest plateau forces appeared at 33 pN and 41 pN for A $\beta$ 1–40 and A $\beta$ 25–35, respectively. The rest of the peaks appeared at forces that are integral multiples of the 33- or 41-pN unit forces.

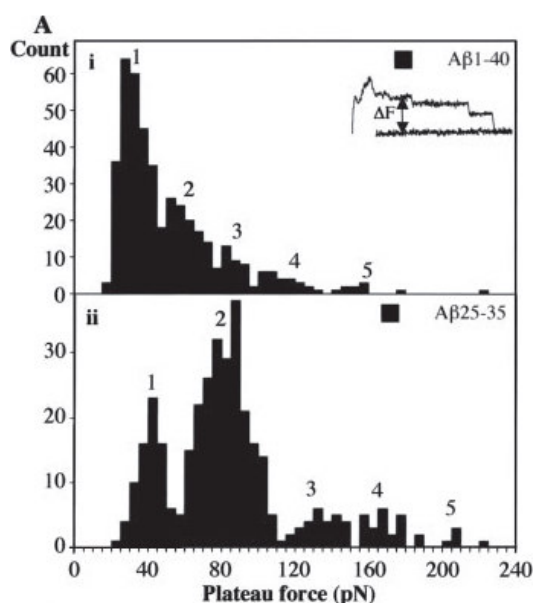


**Fig. 4.** Nanomechanical fingerprint of A $\beta$ -fibrils. Distribution of plateau forces for A $\beta$ 1–40. (**A, i**) and A $\beta$ 25–35 (**A, ii**) fibrils. Numbers above histogram peaks indicate the putative number of elastic strands involved in the transition. **A, i, inset** illustrates the definition of force plateau height.

We observed a significant difference between the unit unzipping forces for A $\beta$ 1–40 and A $\beta$ 25–35 fibrils. The multiple peaks in the plateau force histograms (Fig. 4.) were interpreted to arise from the simultaneous unzipping of strands containing different numbers of  $\beta$ -sheets. Accordingly, the smallest unit forces of 33 or 41 pN correspond to the unzipping of single A $\beta$ 1–40 or A $\beta$ 25–35  $\beta$ -sheets from the fibril, respectively.

At present we can only speculate about the origin of the differences between the unit unzipping forces of A $\beta$ 1–40 and A $\beta$ 25–35  $\beta$ -sheets. Considering that amino acid side chain interactions determine the strength of interaction between parallel  $\beta$ -sheets, the origin of the unzipping force difference could be because of differences in the arrangement of the exposed side chains. One possibility is that Lys-28, which participates in forming a salt bridge with Asp-23 that stabilizes the hairpin structure of the A $\beta$ 1–40 peptide, is exposed in A $\beta$ 25–35 and may form a relatively strong interaction with Met-35 of the neighboring peptide, resulting in greater unzipping forces

### REVERSIBILITY OF FORCE PLATEAU AND FORCE STEP

The lack of force hysteresis often seen in the force responses (Fig. 5) indicates that the mechanically perturbed amyloid fibril system passes through identical structural states during stretch and release and is in thermodynamic equilibrium at each point of extension. The absence of stretch-rate dependence of plateau force (Fig. 5B) indicates that the equilibrium is highly dynamic and the system fluctuates between the (associated and dissociated, or zippered and unzipped) states on a time scale that is much faster than that of the pulling experiment.

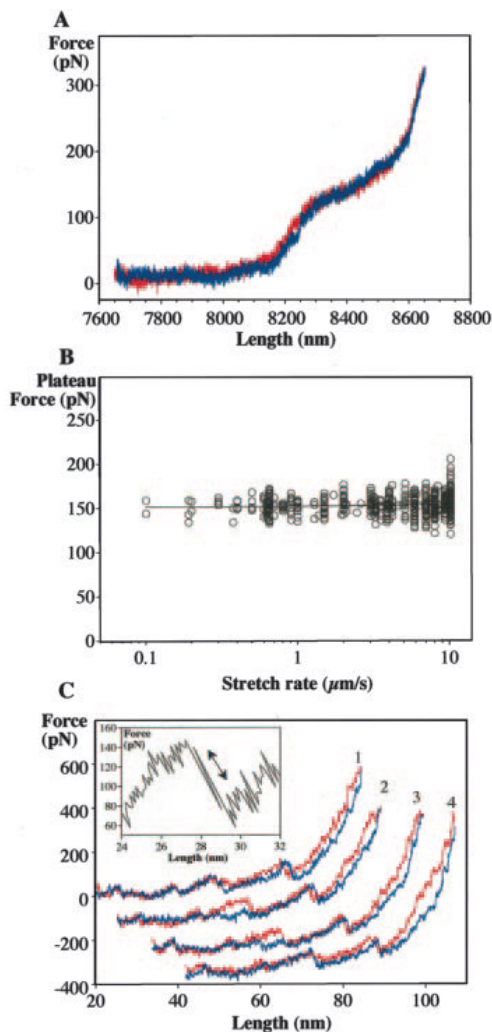


**Fig. 5.** Reversibility and repeatability of the unzipping transition and force staircase. **A**, reversible force plateau, where the plateau is coupled with non-linear elastic response. **B**, plateau force as a function of stretch rate. The plateau force was measured for the same strand stretched repeatedly at different rates. **C**, reversible descending force staircase coupled with non-linear elastic response recorded in four subsequent stretch-relaxation cycles. Inset, enlarged view of the transition showing fluctuations between the high force and low force states (double arrow).

## TIME-DEPENDENT AFM IMAGING AND FORCE SPECTROSCOPY

The force spectroscopy results suggested that during stretch elastic strands are pulled off the A $\beta$ -fibril surface. To explore the nature of these strands, time-dependent AFM imaging and force spectroscopy experiments were performed. Fig. 6. shows the results for A $\beta$ 1–40 fibrils. Shortly after dissolution in PBSA buffer, globular aggregates were present, but filamentous structures were not observed (Fig. 6, Day 0). In the corresponding force spectra an occasional force sawtooth was observed, but force plateaus and complex force patterns were absent. The length of the captured molecular species was 20 nm. The observed mechanical behavior describes most likely the capture, unfolding, and release of oligomers of the A $\beta$ -peptide. Force plateaus, non-linear elastic responses with long contour lengths, and various combinations of these mechanical responses were observed only after the third day and became prominent in preparations more than 1 week old (Fig. 6, Day 7, lower panel). These preparations contained an abundance of mature A $\beta$ -fibrils.

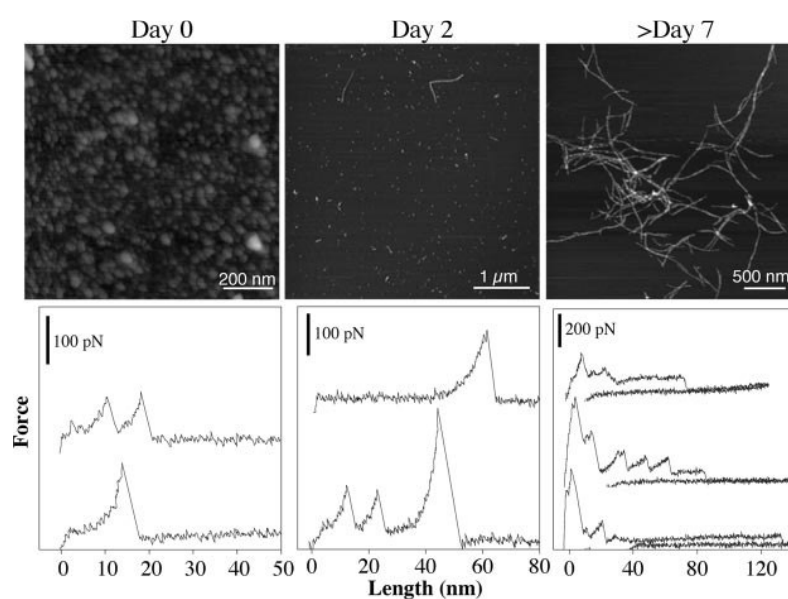


**Fig. 6.** Atomic force microscopy (**upper panel**) and single molecule force spectroscopy (**lower panel**) of A $\beta$ 1–40 as a function of incubation time. Incubation time is shown in days following the dissolution of liophilized peptide (0.5 mg/ml) in PBSA buffer.

Thus, the time-dependent AFM imaging and force spectroscopic results allowed the tentative conclusion that the prominent mechanical responses (Fig. 3) are associated with mature A $\beta$ -fibrils.

# ATOMIC FORCE MICROSCOPY INVESTIGATION OF A $\beta$ 1-42 FIBRILS

## MORPHOLOGY OF A $\beta$ 1-42 AMYLOID FIBRILS

Images of surface-adsorbed A $\beta$ 1–42 fibrils, acquired using non-contact AFM, are shown in Fig. 8. Although the fibrils sometimes had a smooth surface, most often they displayed helical appearance. Fibrils with long helical pitch are shown in Figs. 7A-C. The periodicity in these fibrils was  $108.87 \pm 14.26$  nm (Fig. 7D). We observed a left-handed helical arrangement regardless of the periodicity. The left-handed helices can be particularly well identified in Figs. 7B.

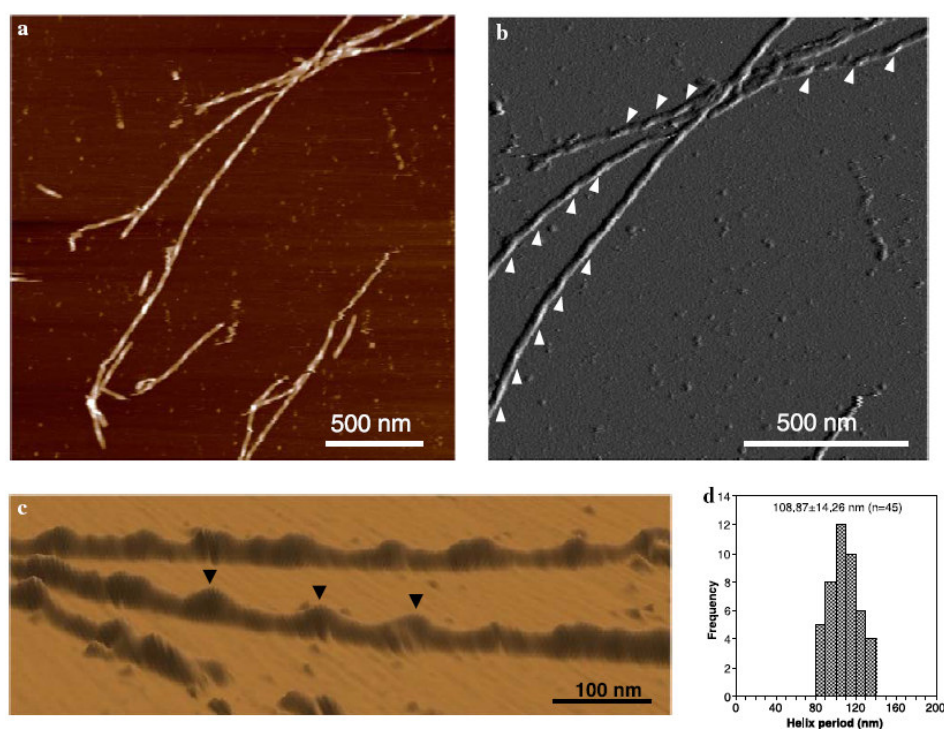


**Fig. 7.** Structural analysis of A $\beta$ 1–42 fibrils with AFM. **A.** Scanning AFM image of A $\beta$ 1–42 amyloid fibrils adsorbed to freshly cleaved mica. Height contrast image collected in non-contact mode in liquid. **B.** An enlarged portion of the image displayed in amplitude contrast. Arrowheads indicate the location and orientation of the helical twist. As evidenced by the image, these fibrils display a lefthanded helical structure. **C.** Three-dimensional rendering of the surface topography of A $\beta$ 1–42 fibrils. Arrowheads indicate periodic height maxima. **D.** Distribution of the distance between neighboring height maxima along the contour of A $\beta$ 1–42 fibrils. The mean spacing is  $108.87 \pm 14.26$  nm.

The mean topographical height of the fibrils, which reflects their diameter, was  $4.77 \pm 1.82$  nm. The height histogram (not shown) displayed multimodal distribution with peaks at approximately 4, 6, 9, and 12 nm.

## VI.2.2 NANOMECHANICAL PROPERTIES OF A $\beta$ 1-42 FIBRILS

Force curves obtained during nanomechanical manipulation of A $\beta$ 1–42 fibrils are shown in Fig. 8. These force curves, which describe a set of molecular characteristics and transitions are referred to as force spectra. Two basic types of force responses could be discerned. The first type of characteristic force response is the force plateau (Fig. 8A), which often occurs as a set of hierarchical force steps (Fig. 8B). The force plateau is characterized by constant force during extension. The plateau typically ends with an abrupt decrease in force. The second type of force response is non-linear elasticity (Fig. 8C). Sometimes fully reversible non-linear stretch and relaxation curves were observed (Fig. 8C).

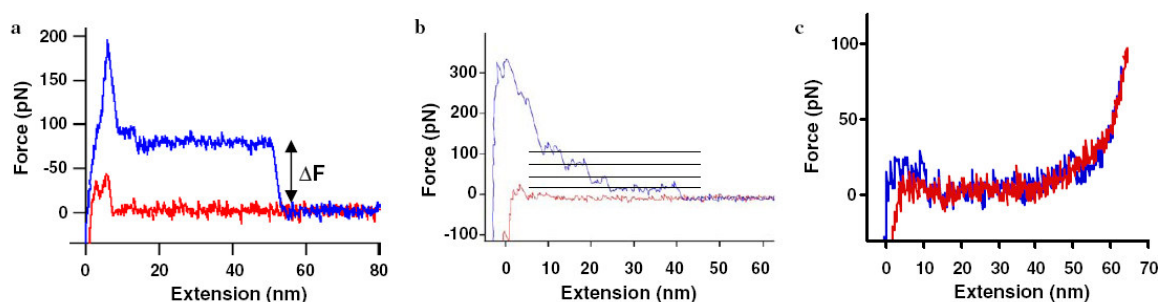


**Fig. 8.** Force versus extension curves of Ab1–42 amyloid fibrils. Stretch and release data are displayed in blue and red, respectively, except where otherwise indicated. **A.** Representative force plateau.  $\Delta F$  marks the height of the force plateau. **B.** Force staircase with contiguous, progressively decreasing force plateaus. Dotted lines mark the plateaus. **C.** Fully reversible, non-linear elasticity.

From the height of consecutive force plateaus a forcestep-height histogram was constructed for the A $\beta$ 1–42 amyloid fibril (Fig. 9) The histogram displayed multimodal distribution with peaks at 23, 45, 70, 90, 110, and 130 pN. For comparison, Fig. 9 also shows the distribution of plateau forces obtained earlier for A $\beta$ 1–40.

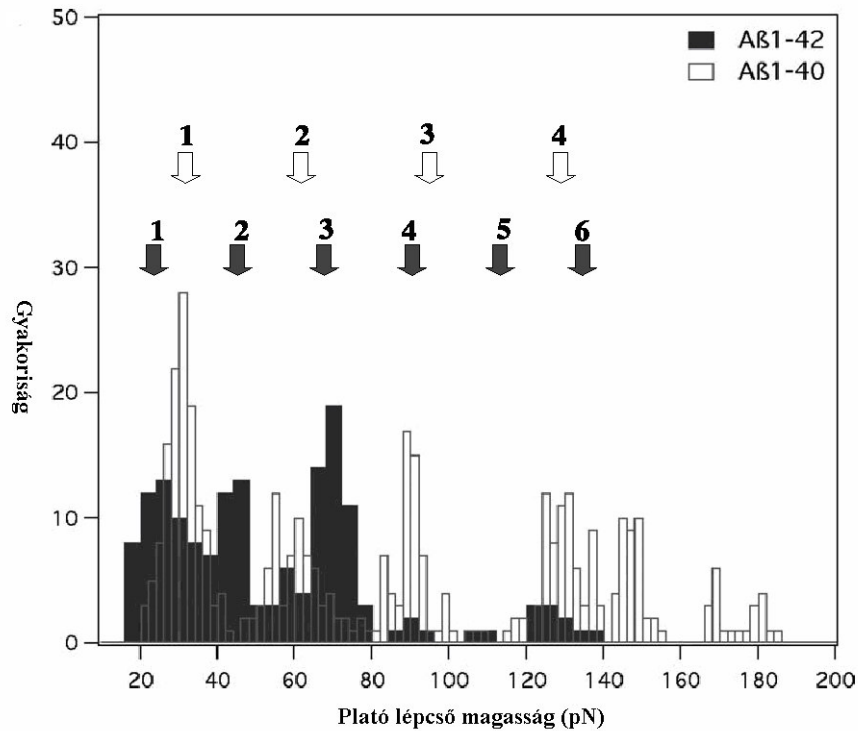


**Fig. 9.** Plateau force step distribution. The plateau force histogram of Aβ1–42 is compared with that of Aβ1–40 . Aβ1–42 and Aβ1–40 histograms are displayed with dark gray and transparent bars, respectively. The numbers and arrows above the histogram peaks indicate the number of Aβ-subunit sheets unzipped in a given force plateau.

## NANOMECHANICAL STABILITY OF THE Aβ25-35\_K28AC FIBRILS

The force spectra of the acetylated Aβ25-35 amyloid fibrils displayed multiple force steps (Fig. 10). The force steps arise as the hierarchical combination and superimposition of several force plateaus. During the force plateau a constant force level is maintained during extension of the molecular system. A force plateau ends with an abrupt, stepwise decrease in force.

The height of the plateau is related to the energy of the bond(s) holding the β-sheets associated to the fibril surface, provided that the system is in thermodynamic equilibrium.

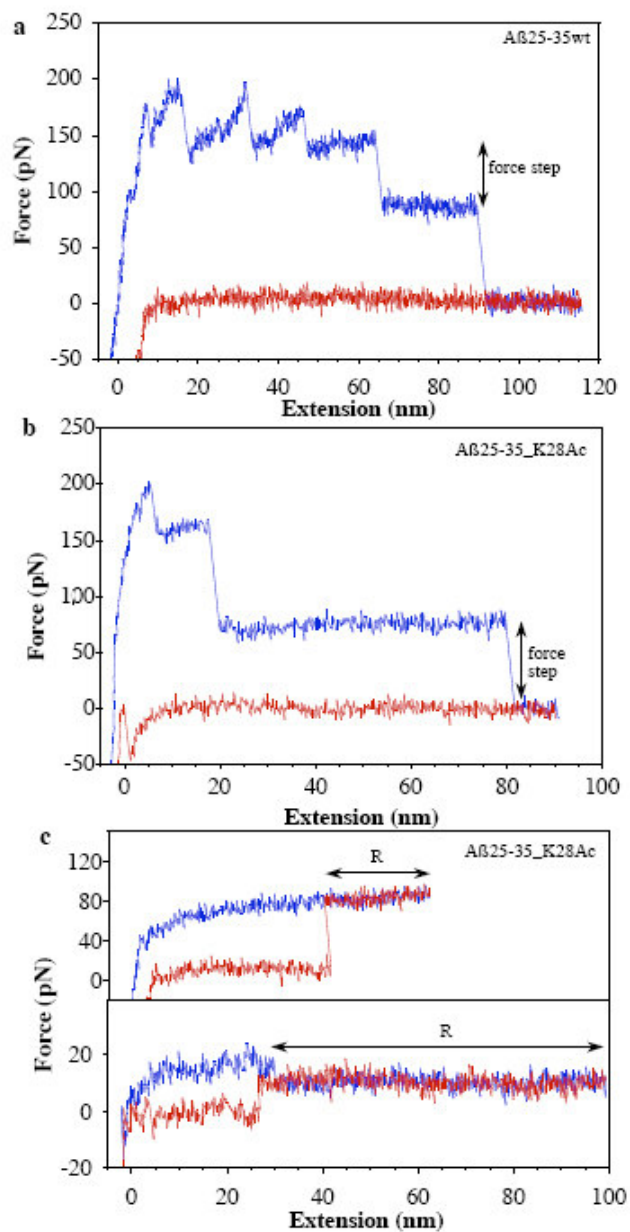


**Fig. 10.** Force spectra of amyloid fibrils. **A.** Force spectrum of A $\beta$ 25-35wt fibril. Lines with two arrowheads mark the concept of the force step analyzed our study. **B.** Force spectrum of A $\beta$ 25-35\_K28Ac fibril. **C.** Examples of reversible force plateaus of A $\beta$ 25-35\_K28Ac fibrils. Reversible regions (R) are indicated with dotted lines with two arrowheads

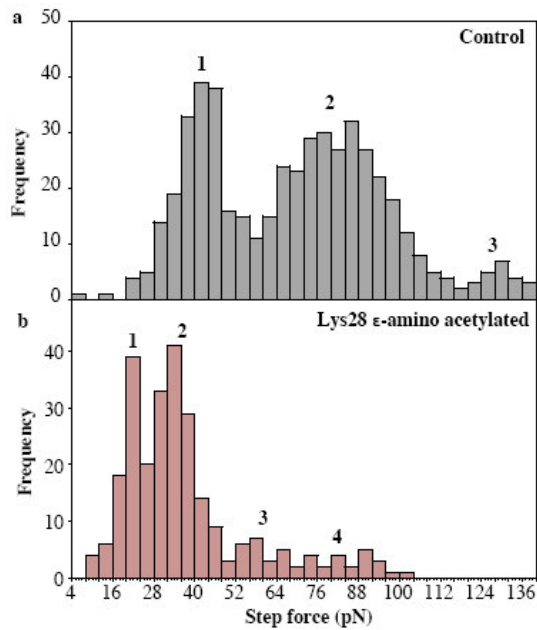


**Fig. 11.** Step force statistics of A $\beta$ 25-35wt **A.** and A $\beta$ 25-35\_K28Ac **B.** The numbers above the histogram peaks indicate the number of  $\beta$ -sheets unzipped.

The force-step histograms displayed multimodal distribution for both A $\beta$ 25-35wt and A $\beta$ 25-35\_K28Ac (Fig. 11.). The histogram peaks appeared at forces that are integer multiples of a fundamental force. The peaks therefore correspond to forces necessary to unzip integer multiples of  $\beta$ -sheets, and the fundamental unzipping force, identified as the lowest-force histogram peak, corresponds to the unzipping force of a single  $\beta$ -sheet. The fundamental unzipping forces were 42 pN and 20 pN for A $\beta$ 25-35wt and A $\beta$ 25-35\_K28Ac, respectively. Thus, significantly lower forces are required to unzip  $\beta$ -sheets formed of the lysine28-acetylated A $\beta$ 25-35 peptide than of the wild type. Presumably, acetylation weakens the interactions of the peptide, and therefore the  $\beta$ -sheet, with its structural neighborhood. One possibility is that the weakening is caused by the abolishment of the positive charge of the Lys28  $\epsilon$ -amino group by acetylation. The electrostatic interaction between the Lys28  $\epsilon$ -amino group and the C-terminus of a neighboring peptide may stabilize the A $\beta$ 25-35 fibril. Lys28 acetylation may therefore abolish the electrostatic stabilization.

# POTASSIUM DEPENDENT ORIENTATED ARRANGEMENT OF A $\beta$ 25-35 FIBRILS ON MICA

## MORPHOLOGY OF A $\beta$ 25-35 FIBRILS ON MICA

It has been shown that charged surfaces interact with A $\beta$ 25–35 suggesting that its binding, and possibly its orientation, may be controlled by electrostatic mechanisms. To explore this possibility, here we investigated the formation of A $\beta$ 25–35 fibrils on a negatively charged mica surface by using AFM methods. Mica is a phyllosilicate, in which Si, Al, P and O atoms are organized into crystalline layers held together by K<sup>+</sup>. On the cleavage surface of mica, hexagonally ordered O ions form K<sup>+</sup>-binding pockets. A $\beta$ 25–35 fibrils displayed a highly ordered trigonal arrangement on a freshly cleaved mica surface (Fig. 12A). There was an angle of 120° between each of the three main orientation directions, which manifested in a regular hexagonal pattern in the 2D FFT image (Fig.12A inset) and 60° between individual fibrils (Fig. 12B).

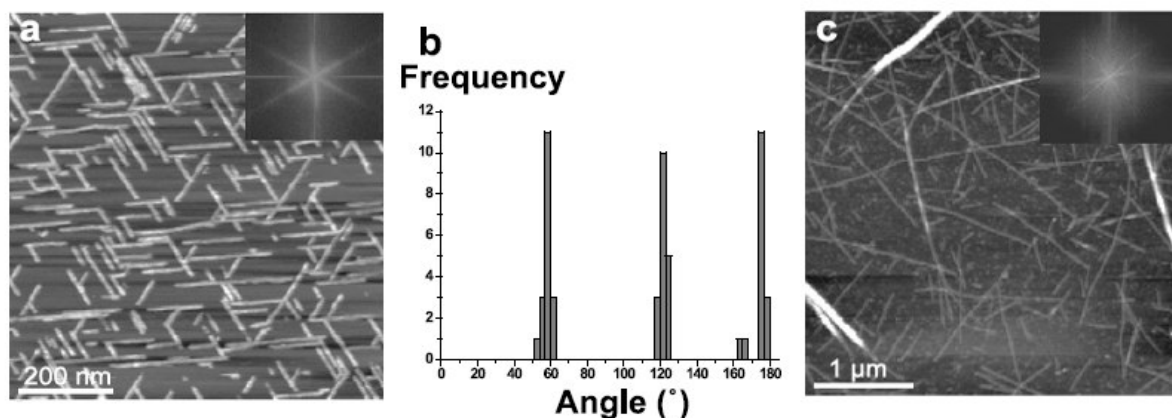


**Fig. 12.** AFM images of A $\beta$ 25–35 fibrils bound to different substrate surfaces. **A.** A $\beta$ 25–35 fibrils on mica. Inset, FFT of the AFM image. **B.** Distribution of orientation angles of A $\beta$ 25–35 fibrils on mica. **C.** A $\beta$ 25–35 fibrils on glass. Inset, FFT of the AFM image.

## EFFECT OF CATIONS

The binding of A $\beta$ 25–35 to mica showed a strong K<sup>+</sup> sensitivity and specificity. In the case of the mica surface pre-coated (at low KCl concentration) with A $\beta$ 25–35 fibrils, the KCl concentration could be increased up to 500 mM and no major fibril dissociation was observed (Fig. 13.). The K<sup>+</sup> sensitivity of binding indicates that A $\beta$ 25–35 peptides compete for the K<sup>+</sup>

-binding pocket on the mica surface. Because K<sup>+</sup>-binding on the mica surface is highly specific due to spatial constraints, other monovalent cations such as Na<sup>+</sup> are less effective in inhibiting A $\beta$ 25–35 binding.

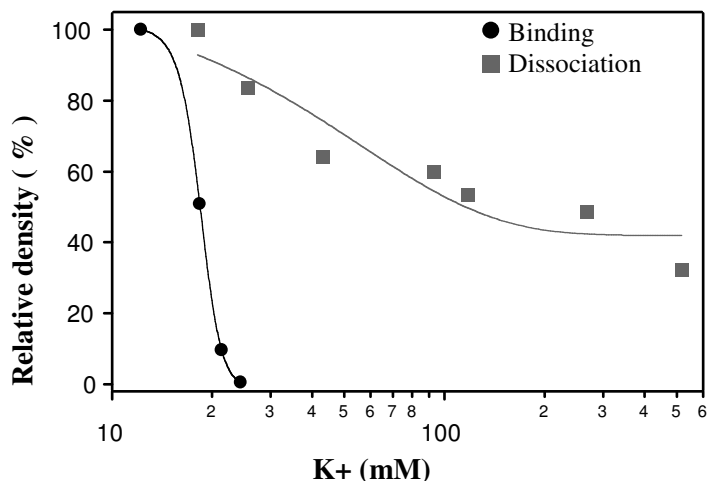


**Fig. 13.** Relative surface density of A $\beta$ 25-fibrils on mica as a function of KCl concentration. The effects on binding and dissociation are compared.

#### **EFFECT OF PEPTIDE ACETYLATION ON ORIENTATION**

To test the role of positively charged groups of A $\beta$ 25–35 in oriented binding to mica we investigated the properties of peptides acetylated on either the N-terminus (A $\beta$ 25–35 G25Ac) or on the  $\epsilon$ -amino group of Lys28 (A $\beta$ 25–35 K28Ac) (Fig. 14.). Notably, the KCl sensitivity of binding was markedly increased for each of the acetylated variants (data not shown). Significant fibril binding to the mica surface was observed only at KCl concentrations below 3 mM. In the case of A $\beta$ 25–35 G25Ac the global trigonal arrangement was maintained (Fig. 14A), but the deviation from the main orientations was increased (Fig. 14D). In the case of A $\beta$ 25–35 K28Ac, the orientation angles differed significantly from those observed for the wild-type (Fig. 14B-C).

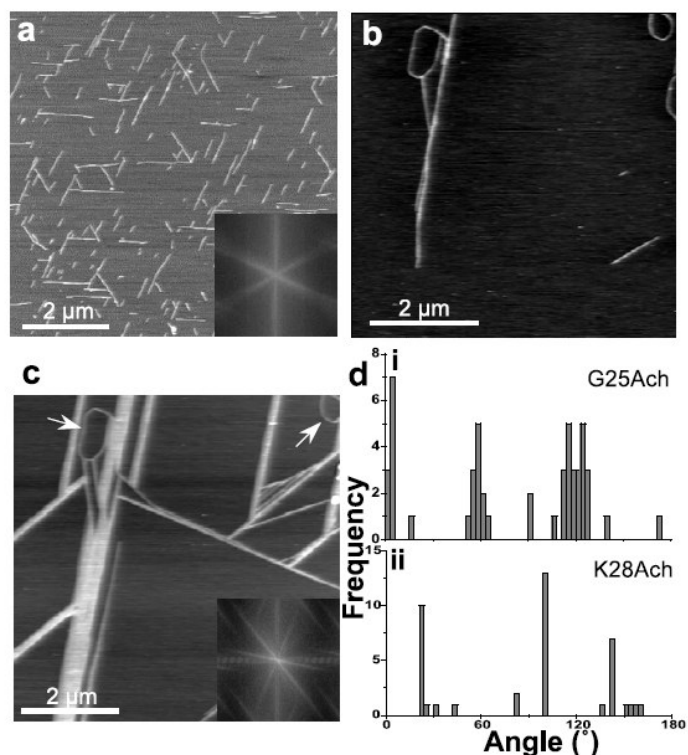


**Fig. 14.** Effect of chemical modification on the orientation of A $\beta$ 25–35 fibrils on mica. **A.** AFM image of A $\beta$ 25–35 fibrils assembled from peptides acetylated on the N-terminus (A $\beta$ 25–35 G25Ac). Inset: FFT of the AFM image. **B.** AFM image of A $\beta$ 25–35 fibrils assembled from peptides acetylated on the  $\epsilon$ -amino group of Lys28 (A $\beta$ 25–35 K28Ac). Fibril arrangement at the initial stages of incubation. **C.** AFM image of A $\beta$ 25–35 K28Ac fibrils on mica after 1 h of incubation. Arrows point at circularly arranged fibrils. Inset: FFT of the AFM image. **D.** Distribution of orientation angles of the fibrils assembled from acetylated peptides. **(i)** Orientation angle histogram for A $\beta$ 25–35 fibrils assembled from peptides acetylated on the N-terminus (A $\beta$ 25–35 G25Ac). **(ii)** Orientation angle histogram for A $\beta$ 25–35 fibrils assembled from peptides acetylated on the  $\epsilon$ -amino group of Lys28 (A $\beta$ 25–35 K28Ac).

Based on our experiments we may conclude that the special spatial arrangement of positively charged groups along the fibril, such as the Lys28 side chain in A $\beta$ 25–35, play fundamental role in the oriented association to the mica surface.

## TEMPORAL EVOLUTION OF ORIENTATION

Time-lapse AFM experiments with A $\beta$ 25–35 peptide in PBS showed that seeds appear on the mica surface from which fibrils grow in the main orientational directions until they hit the side of an already developed fibril, where growth stops (Fig. 15. (upper panel)). Oriented fibrils grew at each of their ends with speeds up to 100 nm/min. Fibril growth proceeded until the fibril end reached a roadblock, typically in the form of another fibril lying across its growth path.

To further dissect the molecular events associated with oriented amyloid growth, we recorded time-lapse AFM images at increased K<sup>+</sup> concentrations (30 mM), which we have previously shown to inhibit fibril binding. Although the binding of new fibrils became strongly inhibited, growth from pre-existing fibril seeds already bound to the surface proceeded, albeit with a reduced velocity (Fig. 15. (lower panel)).

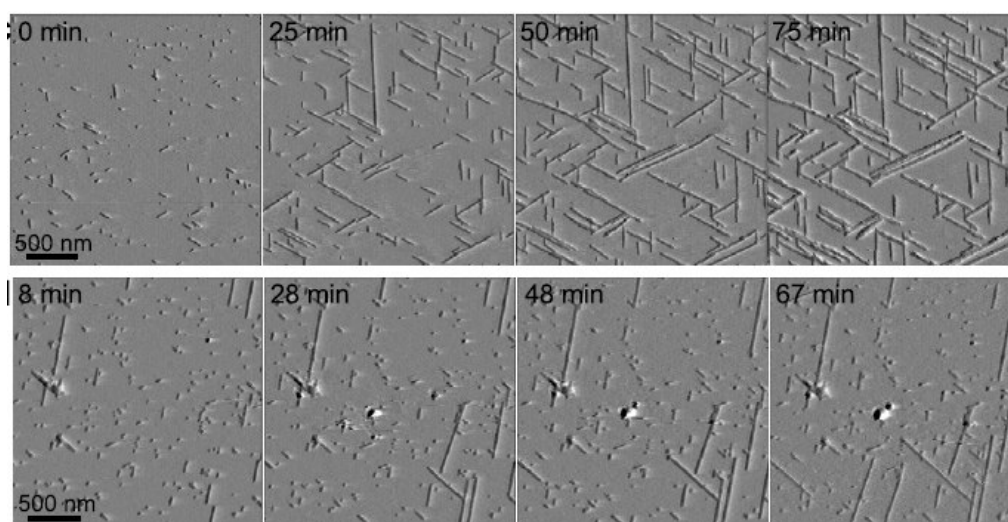


**Fig. 15.** In situ time-lapse AFM of oriented A $\beta$ 25–35 fibril growth. (Upper panel) KCl concentration was 10 mM. Both fibril growth and binding of new seeds are observed. (Lower panel) In situ time-lapse AFM of oriented A $\beta$ 25–35 fibril growth in the presence of 30 mM KCl. The mica surface was pre-coated, for 1 min, with A $\beta$ 25–35 fibrils in 10 mM KCl so as to establish seeds. Subsequently, peptides in the presence of 30 mM KCl were added. Notably, the binding of new seeds is abolished, but growth from existing seeds can be observed.

Thus, oriented A $\beta$ 25–35 fibril formation on mica is likely to involve two different binding events: 1) binding of a peptide unit directly onto the mica surface and 2) binding of a peptide unit to the free end of a pre-existing fibril.

## SCANNING FORCE KYMOGRAPHY

### ASSEMBLY DYNAMICS OF INDIVIDUAL A $\beta$ 25-35 FIBRILS

we explored the assembly dynamics of individual amyloid fibrils during template-assisted growth with exceptional spatial and temporal resolution. We focused on analyzing the dynamics of oriented growth of A $\beta$ 25–25 fibrils on mica. In addition, the aggregation of the full-length amyloid peptide, A $\beta$ 1–42 on graphite was monitored

As revealed by the scanning-force kymograms, A $\beta$ 25–35 fibrils grew on both ends, but the net rate was greater on one of them (fast-growing end). The fast-growing end of different fibrils may point at opposite directions despite identical axial orientation, indicating that polarization is independent of the surface and is probably due to the characteristics of the fibril. Fibrils grew on mica and the surface of an already existing fibril. The assembly dynamics of such fibrils were similar to those of the underlying one. The most prominent feature of the self-assembly dynamics was discontinuous growth (Fig. 16.) Bursts of rapid step-like growth were interrupted with pauses of variable time period. In fact, net fibril growth was achieved via an assembly of consecutive steps and pauses.

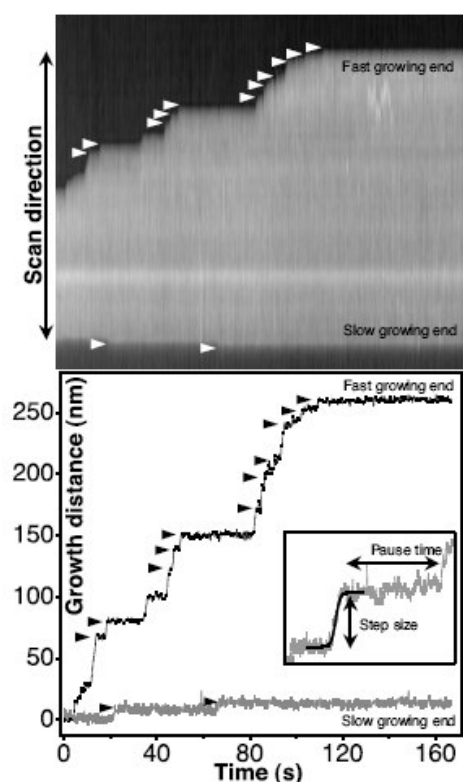


**Fig. 16.** Kymogram (**Upper**) converted to a time-dependent growth–distance plot (**Lower**). White and black arrowheads mark corresponding small growing steps. (**Inset**) Example of sigmoid fit onto a growth step.

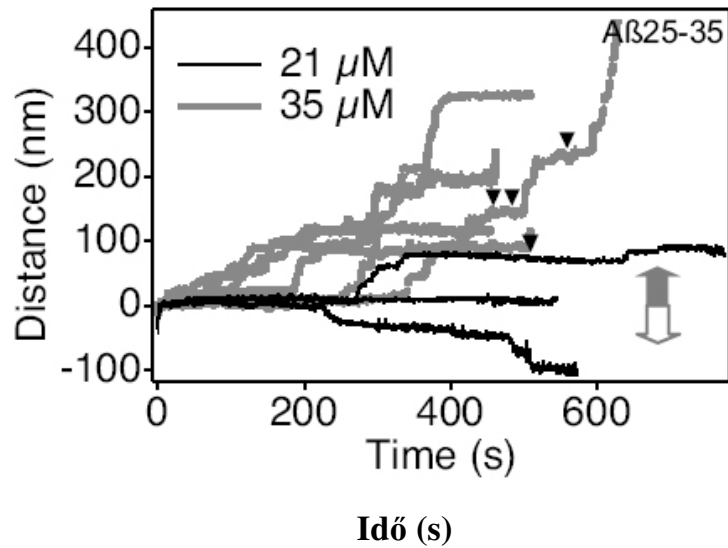


**Fig. 17.** Concentration-dependent kymograms of A $\beta$ 25–35 fibrils, demonstrating stepwise disassembly events. Gray and white block arrows indicate assembly and disassembly directions, respectively. Black arrowheads indicate backstep events.

#### ASSEMBLY DYNAMICS OF INDIVIDUAL A $\beta$ 1–42 FIBRILS

To investigate whether discontinuous dynamics is a general feature of epitaxial amyloid assembly, we examined the formation of fibrils from the full-length A $\beta$ 1–42 peptide on a highly oriented pyrolytic graphite (HOPG) surface. The A $\beta$ 1–42 fibrils have a hexagonal arrangement on HOPG surface.

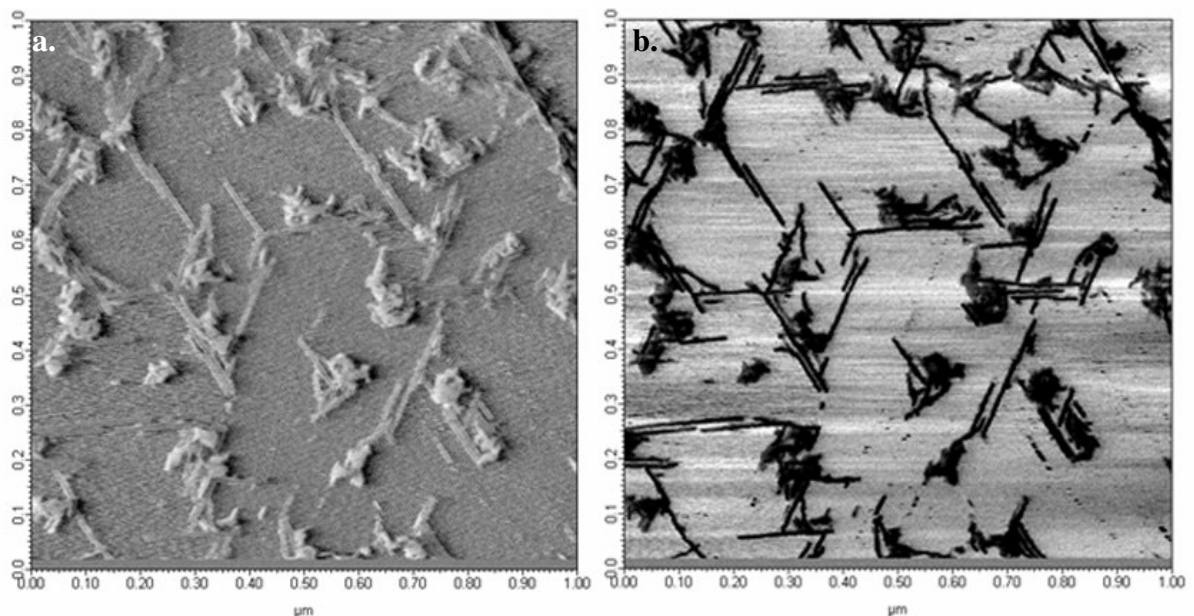


**Fig. 18.** AFM image of hexagonally arranged A $\beta$ 1–42 fibrils on HOPG surface. **A.** Amplitude contrast **B.** Phase contrast.

After a lag phase that lasted up to 60 min, oriented A $\beta$ 1–42 fibrils with lengths up to several hundred nanometers were formed, which maintained a dynamic equilibrium characterized by stepwise length fluctuations. Kymograms of such fibrils (Fig. 19.) contained stepwise assembly and disassembly events and were often dominated by a net disassembly due most likely to the mechanical effect of the scanning AFM tip and to the weak interaction between A $\beta$ 1–42 and graphite. Notably, the net length changes are partitioned according to fast and slow fibril ends, similarly to the A $\beta$ 25–35 peptide.

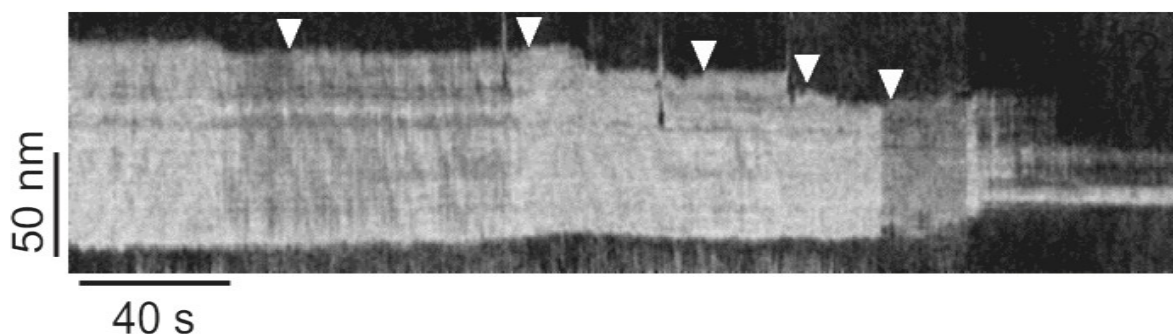


**Fig. 19.** Kymogram of A $\beta$ 1–42 on HOPG, revealing net stepwise disassembly. Grayscale intensity corresponds to the phase shift of the sinusoidally oscillated cantilever. White arrowheads indicate small assembly steps

## GENERAL CONCLUSIONS

1. We characterized the nanomechanical properties and fingerprints of A $\beta$ 1-42, A $\beta$ 1-40, A $\beta$ 25-35 and A $\beta$ 25-35\_K28Ac fibrils. Two fundamental types of mechanical responses were deduced in all type of examined A $\beta$ -fibrils: (a) fully reversible, non-linear elasticity, and (b) characteristic force plateau characterized with a constant force level during stretch. We have mechanically manipulated individual amyloid  $\beta$ -fibrils and argued that their complex mechanical responses are most plausibly explained by a reversible unzipping of long elastic  $\beta$ -sheets from the fibril. The findings are thought to have important implications for understanding the structure, structural dynamics, and mechanisms of formation of amyloid fibrils. The reversible rebinding of  $\beta$ -sheets at high loads and loading rates to the underlying fibril surface indicates that the associated state is strongly favored and a mechanically perturbed amyloid fibril is rapidly recovered by zipping together the  $\beta$ -sheets.
2. We demonstrated that A $\beta$ 25–35 fibrils display a highly ordered trigonal arrangement on mica, which is highly sensitive to K<sup>+</sup> ions. Oriented fibril formation is the result of epitaxial filament growth rather than the binding of fibrils from solution. Mica-driven oriented amyloid fibril growth may have important implications for nanotechnology applications and also for understanding the mechanisms of fibril formation induced by charged surfaces. The oriented fibril arrangement could in principle be utilized to generate regular arrays of amyloid-based nanostructures. By using mutant A $\beta$ 25–35 peptides containing amino acid residues with specific chemical reactivities (e.g. sulfhydryls), oriented arrays of molecular devices (e.g. motor proteins, enzymes) or electrically conducting nanoparticles may be constructed.
3. To explore the dynamics of amyloid self-assembly with high spatial and temporal resolution, we implemented a modified AFM method that we call scanning-force kymography. The method we used, scanning-force kymography, provided a glimpse at the dynamics of individual amyloid fibril self-assembly with unprecedented detail. Considering its simplicity and richness of high-resolution information, the technique may be used to analyze the assembly dynamics of a wide variety of linear biopolymers.

We demonstrated that A $\beta$ 25-35 and A $\beta$ 1-42 fibril assembly and disassembly were not continuous but proceeded in bursts of rapid steps interrupted with pauses that lasted for up

to tens of seconds. The stepwise assembly dynamics suggest that the amyloid fibril fluctuates between structural states in which growth may be either permitted or inhibited.

The observations suggest that amyloid assembly is a highly dynamic process, and the rapid stepwise dynamics may be a general feature of epitaxial amyloid growth.

## PUBLICATIONS

### PAPERS

1. Kellermayer, M.S.Z., Grama, L., Karsai, Á., Nagy, A., Kahn, A., Datki, Z. and Penke, B. Reversible unzipping of amyloid  $\beta$ -fibrils. *J. Biol. Chem.* **280(9)**, 8464-8470, 2005. IF 5,854 (2005)
2. Karsai, Á., Nagy, A., Kengyel, A., Mártonfalvi, Zs., Grama, L., Penke, B. and Kellermayer, M.S.Z. Effect of lysine-28 side chain acetylation on the nanomechanical behavior of Alzheimer amyloid  $\beta$ 25-35 fibrils. *J. Chem. Inf. Mod.* **45 (6)**, 1641-1646, 2005. IF 2.81 (2004)
3. Karsai, Á., Mártonfalvi, Zs., Nagy, A., Grama, L., Penke, B. and Kellermayer, M.S.Z. Mechanical manipulation of Alzheimer's amyloid  $\beta$ 1-42 fibrils. *J. Struct Biol.* **155**, 316-326, 2006. IF 3.49 (2005)
4. Árpád Karsai, László Grama, Ünige Murvai, Katalin Soós, Botond Penke and Miklós S Z Kellermayer  
Potassium-dependent oriented growth of amyloid  $\beta$ 25–35 fibrils on mica  
*Nanotechnology* 2007, 18. 345102 IF.:3,037 (2006)
5. Kellermayer MS, Karsai A, Benke M, Soós K, Penke B.  
Stepwise dynamics of epitaxially growing single amyloid fibrils.  
*Proc Natl Acad Sci U S A.* 2008 Jan 8;105(1):141-4. IF.: 9.643 (2006)

### OTHER PUBLICATIONS

1. Csutora P., Karsai Á., Nagy T., Vas B, Kovács L.G., Rideg O., and Miseta A. Lithium induces phosphoglucomutase activity in various tissues of rats and in bipolar patients  
*Int J Neuropsychopharmacol.* 2005 Nov 1;:1-7 IF: 3,981 (2005)
2. Kiss, B., Karsai, Á. and Kellermayer, M.S.Z. Nanomechanical properties of desmin intermediate filaments. *J. Struct Biol.* **155**, 327-339, 2006 IF 3.49 (2005)
3. Miklós S.Z. Kellermayer, Árpád Karsai, András Kengyel, Attila Nagy, Pasquale Bianco, Tamás Huber, Ágnes Kulcsár, Csaba Niedetzky, Roger Proksch and László Grama. Spatially and temporally synchronized atomic force and total internal reflection fluorescence microscopy for imaging and manipulating cells and biomolecules. *Biohys. J.* 91, 2665-2677, 2006. IF 4.757 (2006)

4. Karsai A, Murvai U, Soós K, Penke B, Kellermayer MS. Oriented epitaxial growth of amyloid fibrils of the N27C mutant beta25-35 peptide. *Eur Biophys J.* 2008 Jan 9 IF.:1,825 (2006)

## IMPORTANT POSTERS

1. Kellermayer, M.S.Z., Grama, L., Karsai, Á., Nagy, A., Kahn, A., Datki, Z. and Penke, B. Reversible unzipping of amyloid  $\beta$ -fibrils. *Biophys. J.* **88**, 198A-199A, 2005.
2. Kellermayer, M. S., Grama, L., Karsai, Á., Nagy, A., Kahn, A., Datki, Z., Penke, B. (2005) Structural dynamics of amyloid explored by manipulating individual fibrils *FEBS Journal* **272** (s1) F2-016P.
3. Miklós S.Z. Kellermayer, Árpád Karsai, Attila Nagy, András Kengyel, Tamás Huber, Zsolt Mártonfalvi and László Grama. Synchronized atomic force and total internal reflection fluorescence microscopy for imaging cells and biomolecules. *Biophys J.* **90**, 2006.
4. Árpád Karsai, László Grama, Attila Nagy and Miklós Kellermayer. Oriented, potassium-dependent binding of amyloid beta25-35 fibrils to mica. *Biophys J.* **90**, 2006.
5. Miklós S.Z. Kellermayer, Árpád Karsai, Margit Benke, Katalin Soós, and Botond Penke. Stepwise assembly dynamics of single amyloid fibrils revealed by scanning force kymography. *Biophys. J.* **92**. 2007.
6. Árpád Karsai, Ünige Murvai, Katalin Soós, Botond Penke, and Miklós SZ Kellermayer. Oriented, Chemically Functionalized Amyloid Network With Controllable Mesh Size For Nanotechnology Applications *Biophys. J.* **94**: 2790. 2008